Heat flux in one-dimensional systems

Vagnon, F. *et al*. (2021) ***Géotechnique Letters*** **11**, 1–11, https://doi.org/10.1680/jgele.20.00122

Relating physical properties to temperature-induced damage in carbonate rocks

F. VAGNON*, C. COLOMBERO†, C. COMINA‡, A. M. FERRERO§, G. MANDRONE‖, R. MISSAGIA¶ and S. C. VINCIGUERRA**

Carbonate rocks have a widespread diffusion in the Earth crust and are extensively used in cultural heritage and buildings. These rocks can be naturally or anthropically exposed to high temperatures. Consequently, relating physical properties to temperature-induced damage is extremely important. Six sets of compositionally and texturally different carbonate rocks, spanning from limestones and marbles to dolomitic marbles, were analysed in this study. Different physical properties, such as porosity, seismic wave velocities and electrical resistivity, were measured before and after thermal treatments with heating/cooling ranges between 105 and 600°C. Microstructural observations and optical analyses were used to investigate how temperature-induced damage affects the physical measured properties of the different microstructures. This integrated approach allowed to define a generalised relationship between physical properties and thermal-induced damage, by way of an induced damage index valid for a broad suite of carbonate rocks.

KEYWORDS: geophysics; rocks/rock mechanics; temperature effects

NOTATION

C_U	uniformity coefficient
c	fitting parameter, depending on the specific rock structure and rock degradation effect
D	damn index
D_{10}	value of the grain diameter at 10% of the cumulative distribution
D_{50}	value of the grain diameter at 50% of the cumulative distribution
D_{60}	value of the grain diameter at 60% of the cumulative distribution
F	formation factor
n	porosity
$P(T)$	physical parameter at temperature T
P_0	reference physical parameter value at 20°C
V_P	P-wave velocity
V_S	S-wave velocity
$\rho_{a,WET}$	apparent resistivity in saturated condition
ρ_{fluid}	resistivity of the saturating fluid
σ	standard deviation

Manuscript received 14 September 2020; first decision 27 January 2021; accepted 1 March 2021.

*Department of Earth Sciences, Università di Torino, Torino, Italy (Orcid:0000-0003-0539-0557).
†Department of Environment, Land and Infrastructure Engineering, Politecnico di Torino, Torino, Italy (Orcid:0000-0001-9818-7464).
‡Department of Earth Sciences, Università di Torino, Torino, Italy (Orcid:0000-0002-3536-9890).
§Department of Earth Sciences, Università di Torino, Torino, Italy (Orcid:0000-0001-8422-6303).
‖Interuniversity Department of Regional and Urban Studies and Planning, Torino, Italy (Orcid:0000-0002-5397-9377).
¶Universidade Estadual Norte Fluminense - Darcy Ribeiro/UENF, Laboratorio de Engenharia e Exploração de Petroleo/LENEP, Macaé - RJ – Brasil (Orcid:0000-0001-6284-6755).
**Department of Earth Sciences, Università di Torino, Torino, Italy (Orcid:0000-0002-6939-3549).

INTRODUCTION

High-temperature gradients drive mechanisms of degradation and weakening of rocks, thus controlling a number of geological processes, engineering applications and cultural heritage (Vagnon *et al*., 2019 and references therein).

Among various rocks, carbonates are widespread diffused and are extensively used in cultural heritage artefacts and buildings. Large crustal volumes of carbonate rocks are naturally exposed to significant temperature increases in areas with anomalous geothermal gradients. The exposure to high temperatures could also be related to engineering applications. Forecasting their physical evolution under temperature gradients is therefore of utmost importance for many fields of rock mechanics.

While numerous studies have investigated the damage-induced processes by temperature effects on carbonate rocks (Heap *et al*., 2013; Castagna *et al*., 2018 and reference therein), less attention has been paid to quantitatively generalise throughout physical parameters evolution of the thermal degradation induced by heating.

A relationship linking physical parameters and temperature (thermal degradation relationship) has been proposed by several authors (e.g. Koca *et al*., 2006; Dwivedi *et al*., 2008; Zhao *et al*., 2012; Musso *et al*., 2015; Weydt *et al*., 2018; Vagnon *et al*., 2019) under the form:

$$P(T) = P_0 e^{\pm cT} \quad (1)$$

where $P(T)$ is a given physical parameter at temperature T, P_0 is its reference value at 20°C and c is a fitting parameter, depending on the specific rock structure and rock degradation effect. The sign of the exponent is positive if the considered parameter increases with temperature (negative otherwise). Based on experimental tests, several authors

(Koca *et al.*, 2006; Dwivedi *et al.*, 2008; Zhao *et al.*, 2012; Vagnon *et al.*, 2019) have proposed similar exponential equations for the thermal degradation relationship with a different c fitting parameter.

This study has the main objective of defining a general relationship between physical properties and thermal-induced damage, by way of a multiparametric-induced damage index valid for a broad suite of carbonate rocks.

Six sets of different carbonate rock specimens were tested before and after thermal treatment, with heating/cooling cycles from 105 to 600°C. Density in dry and saturated conditions, porosity, ultrasonic pulse velocity (UPV) and electrical resistivity (ER) were measured. Microstructural observations and both grain-size distribution curves and crack densities were analysed. A unified multiparametric thermally induced damage coefficient was quantified to provide a general law for carbonate rocks.

SAMPLE SETS AND EXPERIMENTAL METHODS

Cylindrical samples obtained from the four different sampling areas (Fig. 1), were classified into six sets:

- Seven limestone samples, coming from the fossil hydrothermal system of Las Minas (Mexico), named 'RLM' in the following.
- Ten dolomitic marble samples, coming from Granados Quarry (Tatatila, Mexico), named 'GQ'.
- Eleven marble samples, coming from San Lorenzo Quarry (Italy), named 'Valdieri'.
- Eighteen marble samples, coming from Italva Basin (Brazil), divided into three subsets (of six specimens, respectively) and named 'Brazil C', 'Brazil D' and 'Brazil SJ'.

Samples diameter ranged from 40 to 50 mm, and the average length of 95 mm. Samples followed the geometric

Fig. 1. Location of the four sampling areas and pictures of the different sets of specimens

Table 1. Percentage of mineral compounds and oxides retrieved from XRD and XRF analyses

	Compound name	RLM	GQ	Valdieri	Brazil C	Brazil D	Brazil SJ
		Concentration: %					
XRD	Calcite	97·3	—	98	37·9	48·98	14·84
	Quartz	2·7	—	—	—	—	—
	Dolomite	—	100	2	42·58	42·46	73·33
	Forsterite	—	—	—	18	—	—
	Tremolite	—	—	—	1·47	—	2·02
	Wairauite	—	—	—	0·05	—	4·61
	Siderite	—	—	—	—	—	5·18
	Olivine	—	—	—	—	8·1	—
XRF	Magnesium oxide	1·106	36·331	2·05	17·33	20·39	21·36
	Calcium oxide	96·529	62·495	97·02	78·84	67·37	76·45
	Silicon dioxide	1·047	0·48	0·425	3·65	11·36	1·898
	Aluminium oxide	0·356	0·118	0·18	—	0·54	—
	Potassium oxide	0·33	0·195	—	—	—	—
	F	0·3	—	—	—	—	—
	CoO	—	0·149	—	0·014	—	0·006
	Ferric oxide	0·131	—	0·13	0·05	0·26	0·17
	Others	0·21	0·233	0·195	0·104	0·0725	0·107

requirements for standard determination of the analysed physical properties.

To analyse the chemical content of each set, x-ray fluorescence (XRF) and x-ray diffraction (XRD) analyses were conducted (Table 1). It can be observed that RLM and Valdieri samples are mostly calcitic (97·3 and 98%, respectively) while GQ samples are essentially dolomitic. Brazilian samples show transitional compositions between these end members.

Following the experimental procedure detailed in Vagnon *et al.* (2019), density in dry and saturated conditions, porosity (n), P- and S-wave velocity (V_P and V_S) and ER (in saturated conditions, $\rho_{a,WET}$) of the 46 core specimens were measured before and after heating (at target

Table 2. Experimental instruments, international standards and main physical parameters

Physical property	International standard	Test instrument	Technical parameters
Density in dry and saturated conditions, Porosity	ISRM (1979). Suggested methods for determining water content, porosity, density, absorption and related properties and swelling and slake-durability index properties. 1977	Caliper Analytical balance	Resolution: 0·0002 m Resolution: 0·0001 kg
P- and S-wave velocity, V_P and V_S	ASTM D 2845-08 (ASTM, 2008)	Ultrasonic pulse generation and acquisition system (Pundit Lab, Proceq)	Two cylindrical 250-kHz tx-rx probes
ER measurement, ρ_{app_dry}	—	Syscal-Pro (Iris instruments) acquisition system	On-purpose built measuring quadrupole (Vagnon *et al.*, 2019)
Heat treatment	—	Carbolite Temperature programmer Eurotherm 2416CG	Temperature range: 1100°C Heating rate: 0·06°C/s Resolution: 1°C
		XRF: S2 Ranger (Bruker Company)	

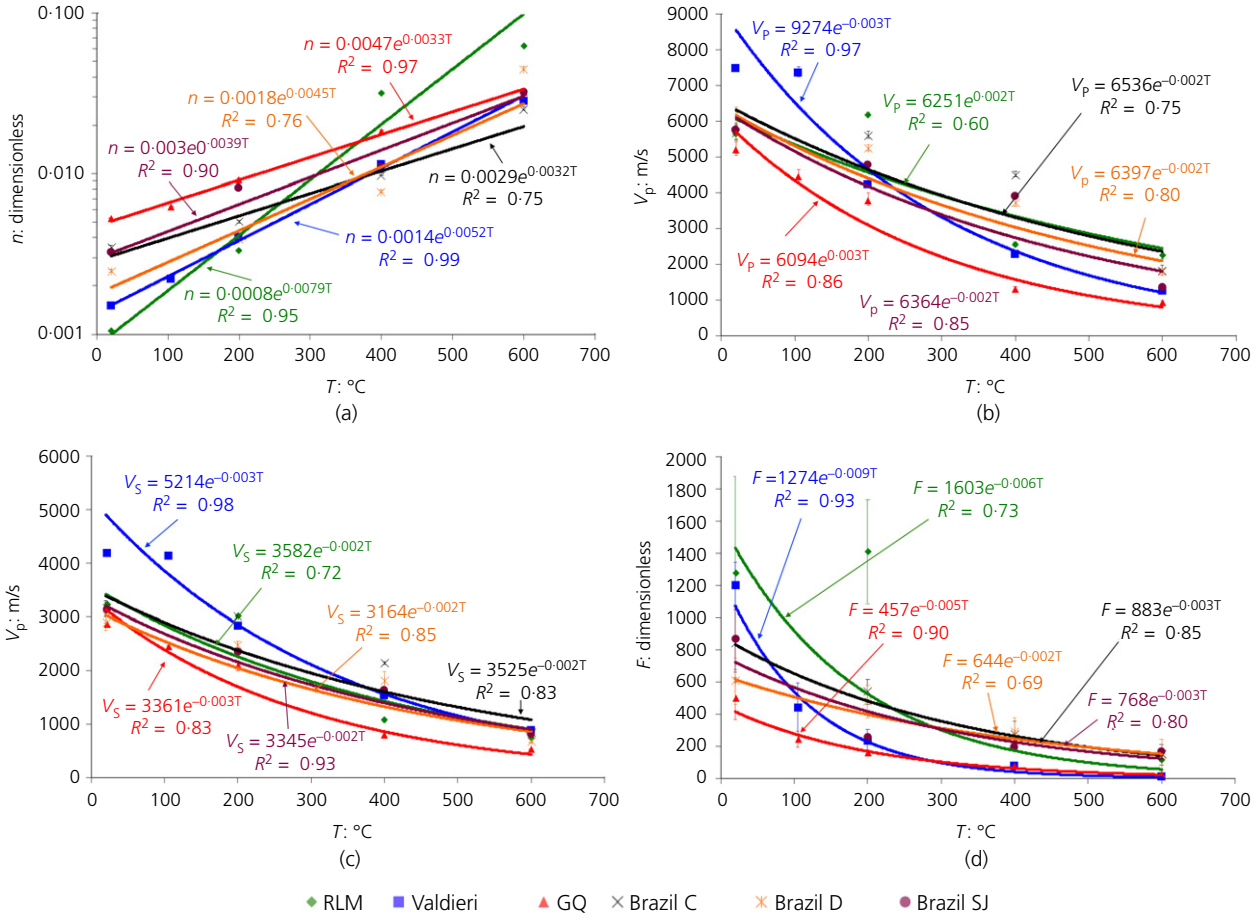

Fig. 2. Relationship between (a) porosity; (b) P-wave velocity; (c) S-wave velocity and (d) formation factor and temperature for the studied samples. All the data are associated to their standard deviations: where not visible, the length of the error bars is lower than the marker size

temperatures of 105, 200, 400 and 600°C, respectively). Table 2 summarises the measured parameters, the international standards and experimental methodologies adopted for their determination. The thermal treatment involved a three-stage procedure (Vagnon *et al.*, 2019): (*a*) sample heating up to the target temperature with a heating rate of 0·06°C/s; (*b*) 24 h sample exposure to constant target temperature; (*c*) slow-rate sample cooling down to room temperature (one day on average). The exposure time allows the uniform heating of the samples, ensuring that the surface temperature was the same inside the sample. Even in cooling phase, the time inside the furnace prevents thermal shocks that may influence the sample physical properties, by increasing the thermal degradation effects.

Values of $\rho_{a,WET}$ were also expressed in terms of formation factor, F (Archie, 1942), a dimensionless parameter that represents the ratio between $\rho_{a,WET}$ and the saturating fluid resistivity, ρ_{fluid}.

To analyse the main effects of thermal treatment on the micro-structure of the studied carbonate rocks, 20 × 40 mm thin sections were obtained from natural and thermal-treated extra-samples belonging to the different

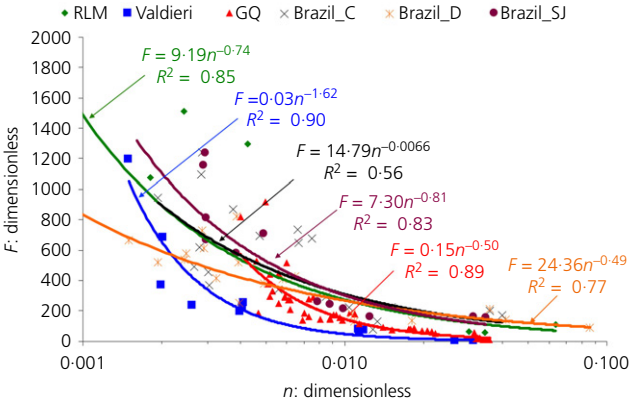

Fig. 3. Relationship between formation factor and porosity for the studied samples. All the data are associated to their standard deviations: where not visible, the length of the error bars is lower than the marker size

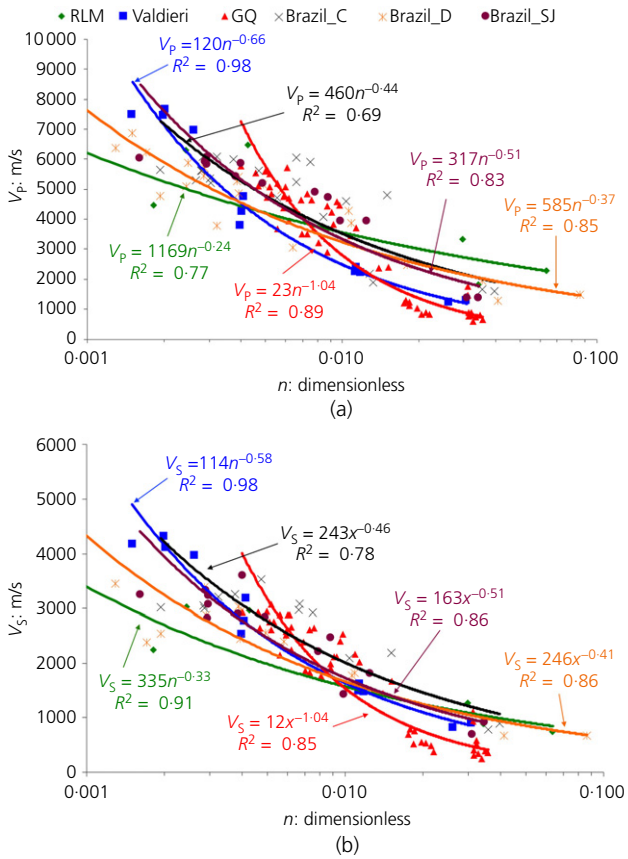

Fig. 4. Relationship between P-wave (a) and S-wave (b) velocity and porosity for the studied samples

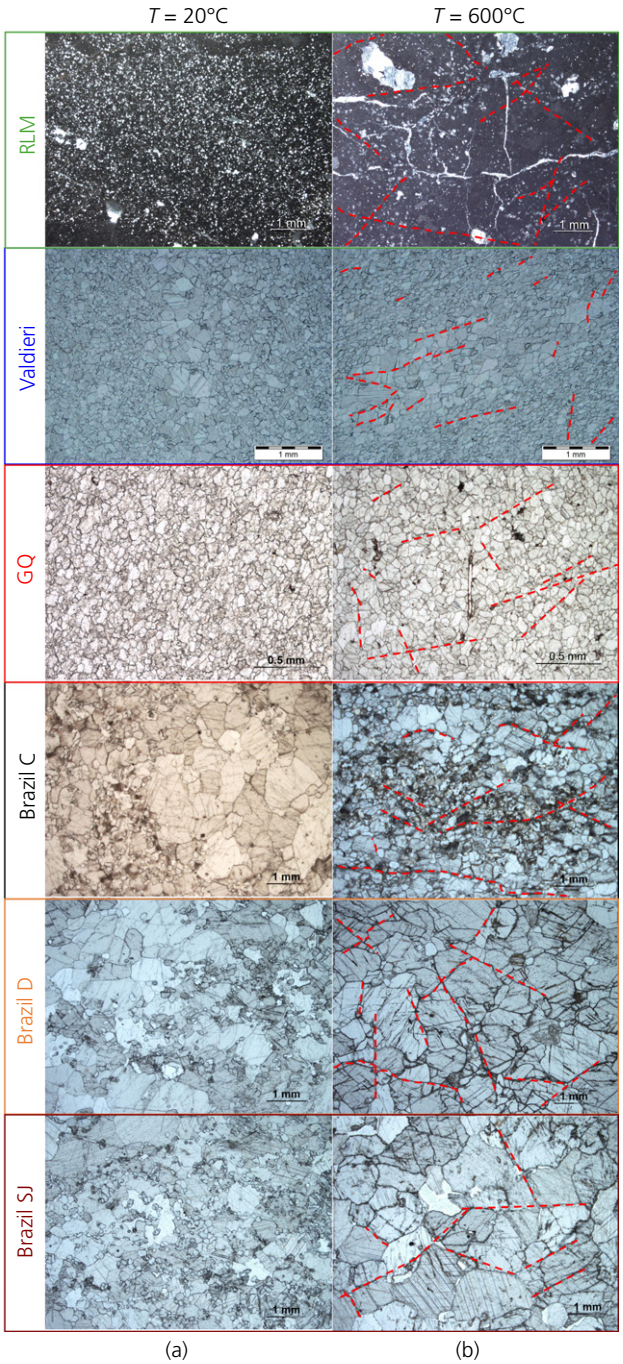

Fig. 5. Optical microscope observations of specimens at 20°C (left column) and at 600°C (right column) and highlight of major thermal cracks generated after thermal treatment (red dashed lines)

sets. Microstructural observations were then performed using a transmitted polarised light microscope. By using the image processing program ImageJ (Schneider *et al.*, 2012), the pre- and post-heating grain-size distribution and crack length (Arganda-Carreras *et al.*, 2010) were measured on thin sections. Crack density, expressed as the ratio between total cracks length and area investigated, was also proposed as a parameter for evaluating thermal damage.

RESULTS

Physical parameter measurements

The thermal treatment induced significant changes in physical properties such as n, UPV and $\rho_{a,WET}$ values for each set of specimens. In Appendix A and Fig. 2 all data are shown. Exponential relationships were fitted to all parameters for each data set, except density values which do not exhibit a clear dependence to the temperature, in agreement with other previous findings (Ferrero & Marini,

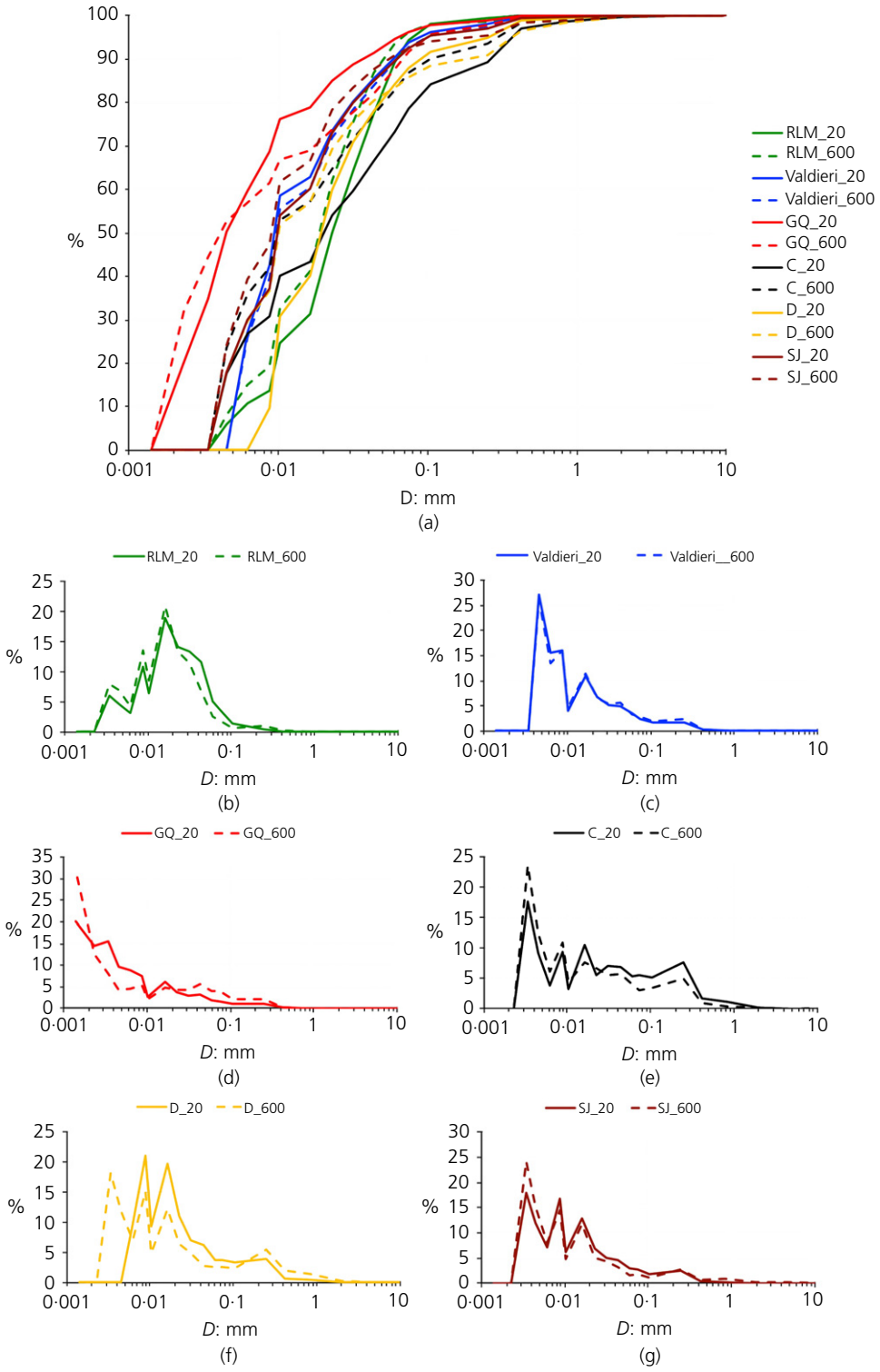

Fig. 6. Cumulative (a) and derivative (b to g for each sample) grain-size distributions of microphotographs at 20°C (continuous lines) and at 600°C (dashed lines)

2000; Koca *et al.*, 2006; Yavuz & Topal, 2007; Peng *et al.*, 2016; Su *et al.*, 2018; Vagnon *et al.*, 2019).

Porosity (Fig. 2(a)) showed an exponential trend with temperature for each set of specimens. In particular, the porosity of RLM limestones was more sensitive to temperature gradients than the other sets of tested specimens.

In general, all the sample sets exhibited the same trends of V_P and V_S with increasing target temperature (Figs. 2(b) and 2(c)), but with initial P- and S-wave velocity values significantly different.

The formation factor values (F) of each individual set of rock samples is reported in Fig. 2(d). A clear modification in electrical properties is found between different rock samples, with increasing target temperature. In particular, F clearly decreased by increasing temperature.

Discussion and relationships between physical parameters

The previous section has highlighted a strong dependence of each single physical parameter on temperature, repeatable

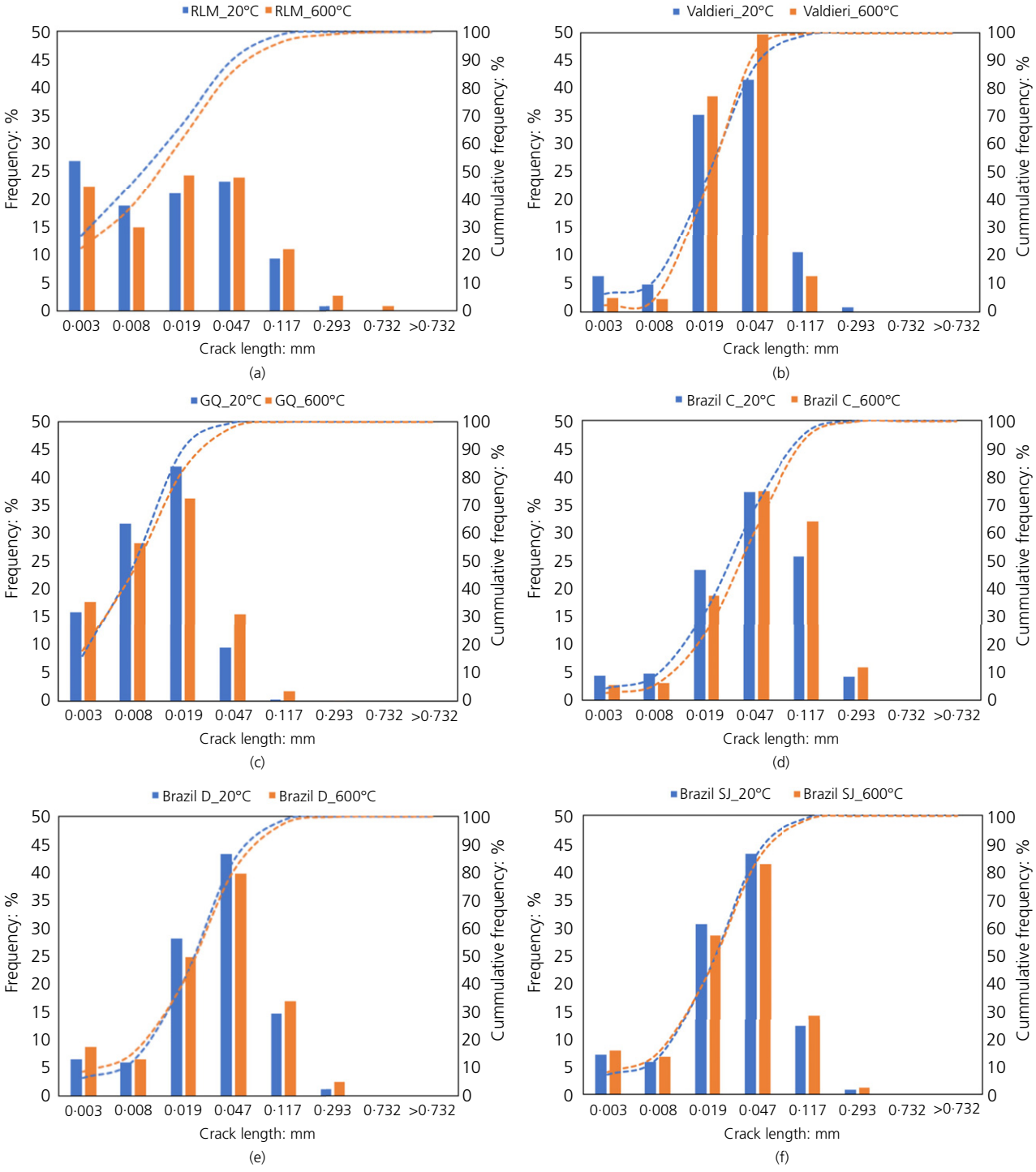

Fig. 7. Frequency (column bars) and cumulative (dashed lines) distribution of crack length for each sample at 20°C (blue) and at 600°C (orange) for each analysed sample (a) to (f)

Table 3. Summary of grain-size distribution performed on micrographs of the tested rocks

Set	T: °C	D_{50}: mm	C_U: –
RLM	20	0·0227	5·05
	600	0·019	5·04
Valdieri	20	0·009	2·20
	600	0·009	3·26
GQ	20	0·0045	3·65
	600	0·004	5·80
Brazil C	20	0·0227	6·96
	600	0·01	4·44
Brazil D	20	0·019	2·61
	600	0·01	4·22
Brazil SJ	20	0·0102	3·62
	600	0·0087	2·27

Table 4. Summary of crack length results performed on micrographs of the tested rocks

Set	T: °C	Crack length: mm			Crack density: 1/mm
		Min	Max	Median	
RLM	20	0·003	0·219	0·009	32·376
	600	0·003	0·898	0·012	42·015
Valdieri	20	0·003	0·303	0·020	28·896
	600	0·003	0·258	0·024	37·444
GQ	20	0·001	0·090	0·008	47·362
	600	0·001	0·136	0·008	49·994
Brazil C	20	0·003	0·672	0·029	12·195
	600	0·003	0·553	0·036	16·182
Brazil D	20	0·003	0·603	0·022	14·120
	600	0·003	0·739	0·023	15·560
Brazil SJ	20	0·003	0·552	0·021	12·444
	600	0·003	0·718	0·022	15·951

for all lithologies investigated. The main findings can be summarised as follows:

- The thermal treatment induced a moderate increase in porosity due to generation of new cracks or re-opening of existing ones at temperatures up to 550°C. At higher temperatures, the porosity increase was likely related to decalcination and decarbonation, leading to increased pore space due to the combination of grain comminution and crack damage (Heap *et al.*, 2013). RLM samples showed a more marked increment in porosity compared to the other samples mirroring the fact that limestones undergo more pronounced textural changes, while marbles, already exposed to high temperatures in their formation history that has led to recrystallisation, maintain a memory of the thermal stresses.
- The increase in porosity is mirrored by a decrease in P- and S-wave velocity and resistivity. With respect to this Valdieri samples showed a slightly different behaviour, since velocities remained relatively constant until 200°C with a significant increase only for higher temperatures. This can be correlated to the presence of dolomite that has been observed (Heap *et al.*, 2013) to strengthen rocks at low temperatures, while decarbonation leads to degradation at higher temperatures.
- Figures 3 and 4 show the inverse power-law relationships between physical parameters and porosities. For the n–V_P and n–V_S relationships, the general degradation of physical parameters also influenced the mechanical characteristics of rock samples. For n–F relationship that represents Archie's law, the determined parameters for the power law are not in agreement with typical observed values for carbonate rocks (e.g. Ara *et al.*, 2001). However, the application of this relationship to carbonate rocks has been already recognised to be difficult due to the complexity of their voids space (e.g. Talabani *et al.*, 2000).

Microstructural observations

Even if micrographs of thin sections cannot be considered completely as representative of the whole volume of the analysed rock samples, their analysis can be very important for identifying how micromechanical damage induced by heating took place. In this respect, Fig. 5 shows micrographs of thin sections before (a) and after thermal treatment (b) at the highest temperature – that is, 600°C, for all lithologies investigated. After heating at 600°C, grain expansion leading to crack generation along grain boundaries is observable in all the samples (Fig. 5). Grain-size analyses can also be considered as a good indicator of the thermal effects, given that the decalcination process can reduce the average grain size at high temperature (Heap *et al.*, 2013). Moreover, the propagation of intragranular microcracks can have a double effect either on the crushing of existing grains or the increase in void volume. For these reasons, both grain-size distributions (Fig. 6) and crack length (Fig. 7 and Table 4) of each micrograph of Fig. 5 were evaluated using the ImageJ code. Moreover, the values of the grain diameter at 50% of the cumulative distribution (D_{50}), the uniformity coefficient (C_U), obtained as the D_{60}/D_{10} ratio and the crack density were additionally determined (Tables 3 and 4).

The analyses highlighted that:

- The temperature increase generates a shift of the grain-size distributions to smaller values, strengthening the hypothesis of the formation of microcracks inside initial bigger grains.
- RLM and Valdieri samples experienced higher thermal degradation since they exhibit the highest increase in crack density. For RLM samples this is probably due to the fact that limestone underwent deeper textural changes with respect to metamorphic rocks or carbonates already affected by high-temperature gradients and circulation of high-temperature fluids.

TOWARDS A UNIFIED DAMAGE INDEX

From the above reported results, an induced damage index for carbonate rocks exposed to different temperatures can be proposed. For porosity, the induced damage index can be defined as:

$$D_n = 1 - \frac{n_{RT}}{n(T)} \tag{2}$$

where D_n is the induced damage index for porosity, n_{RT} is the room-temperature porosity and $n(T)$ is the porosity evaluated at the different target temperature.

For the other parameters the induced damage index can be written as

$$D_{pP} = 1 - \frac{P(T)}{P_0} \tag{3}$$

where D_P is the induced damaged index for the generic parameter.

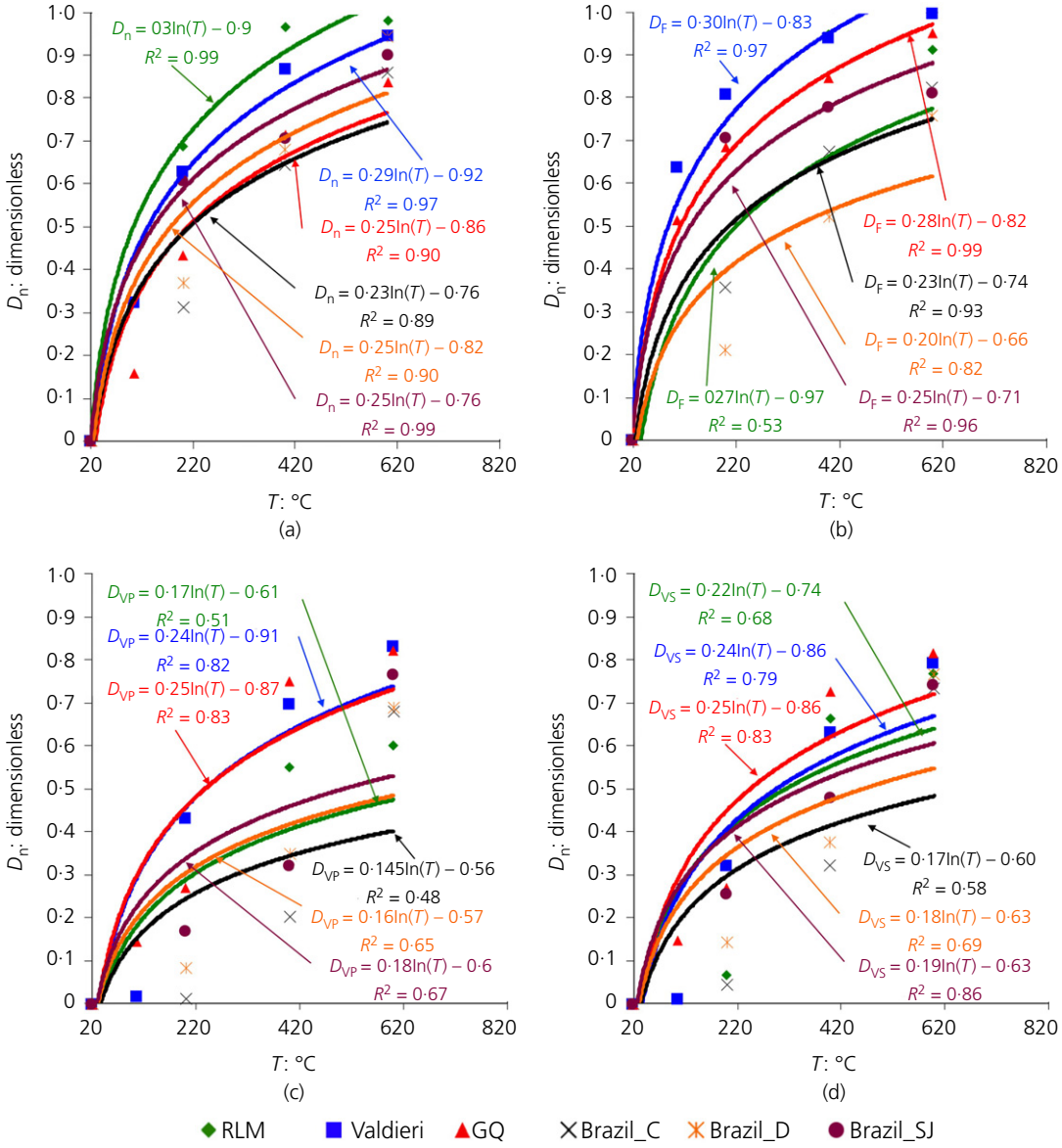

Fig. 8. Relationship between the induced damage index for (a) porosity; (b) formation factor; (c) P- and (d) S-wave velocity and temperature

The variation of damage index with temperature is shown in Fig. 8 for each considered parameter. In general, damage indexes gradually increase with temperature following a logarithmic distribution. A dependence on the lithotype is also noticeable in terms of absolute values, while the relative trends remain comparable (Fig. 8). The most plausible explanation may be found in the interplay of bulk composition and strength (dolomitisation and/or grains recrystallisation) and degree of cementation.

The significance of the proposed damage index formulation for carbonatic rocks was assessed by comparing the experimental data with companion results available from literature (Ferrero & Marini, 2000; Sengun, 2013; Yavuz *et al*., 2010; Brotóns *et al*., 2013; Zhang *et al*., 2017). Figure 9 shows the thermal damage trends for fine marble, coarse marble and dolomitic marble (respectively fuchsia dotted, continuous and dashed lines) and limestone (black continuous line) for n (Fig. 9(a)) and V_P (Fig. 9(b)). The trends were evaluated by combining equation (2) (for n) and equation (3) (for V_P) with equation (1) and considering c equals to the fitting parameters shown in Fig. 2. It is possible to see that the experimental results obtained by the majority of the studies fall into these domains, proving the goodness of the proposed unified damage index. However, specific parameter calibration within the proposed limits should be performed for the different materials.

CONCLUSIONS

A series of laboratory tests on six, compositionally and texturally different, carbonate rocks was performed to investigate the variation of multiple physical parameters as a function of increasing temperature.

The main findings of this study can be summarised as

- In the range 200–400°C, a turning point in the trend of physical behaviour is identified.
- The effect of temperature on physical properties depends mainly on rock texture, bulk composition and grain-size distribution resulting from the interplay of the primary processes of rock formation and recrystallisation.
  In particular, if the rock was already naturally exposed to high temperatures, a stress memory is preserved and only minor changes in the physical parameters were detected

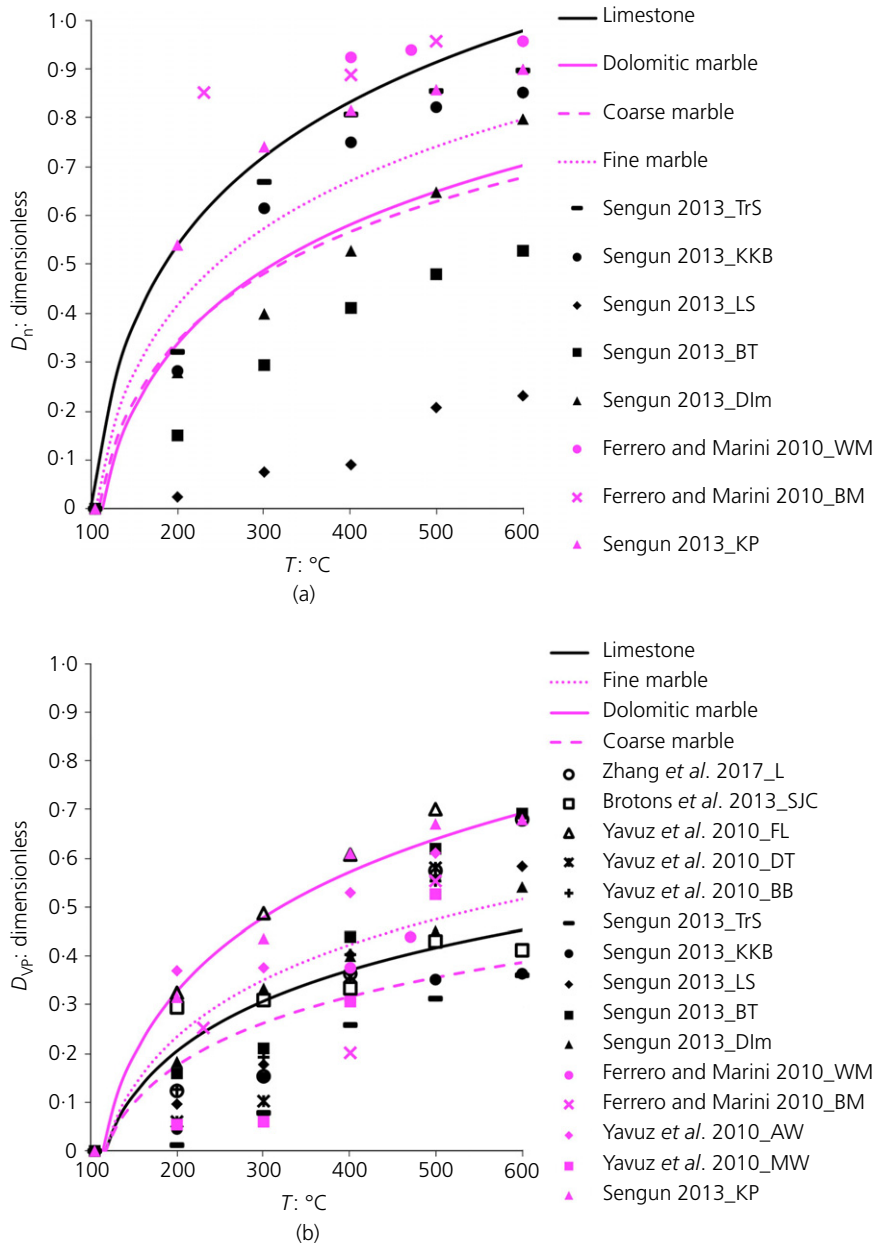

Fig. 9. Comparison between the proposed damage index and published results for porosity (a) and P-wave velocity (b). The results were grouped according to the rock type (black markers and lines for limestones and fuchsia for marbles). The acronym near the author's names stands for the material type (L: Linyi limestone; SJC: San Julian's calcarenite; FL: Finike Lymra limestone; DT: Denizli travertine; BB: Burdur Beige limestone; AW: Afyon White marble; MW: Mugla White marble; Dlm: Balikesir-Marmare Isaland Dolomitic limestone; TrS: Kayseri-Develi limestone; KKB: Burdur-Yesilova limestone; LS: Antalya-DEmre limestone; BT: Burdur-Bucak travertine; KP: Afyon-Ischisar marble; BM: Ormea Black marble; WM: Perlato Sicilia marble)

after thermal treatment. As a consequence, limestone samples exhibit a much higher thermal damage compared to marbles already exposed at high temperature and circulation of fluids at high temperature, especially in terms of porosity increase.

- A ubiquitous exponential relationship between physical parameter and temperature was found for each considered carbonate rock, where the exponent c (equation (1)) can have positive or negative sign:
  - $c = 0{\cdot}0044 \pm 0{\cdot}003$ for limestone;
  - $c = 0{\cdot}0035 \pm 0{\cdot}0021$ for fine grain marble;
  - $c = 0{\cdot}0026 \pm 0{\cdot}0006$ for coarse grain marble;
  - $c = 0{\cdot}0036 \pm 0{\cdot}001$ for dolomitic marble.

These coefficients were calculated as the average of the c values of each rock set considered in this paper.

- A unified coefficient D for quantifying the thermal damage of carbonate rocks has also been proposed and compared with available data from literature.

CONFLICTS OF INTEREST

The authors declare that there is no conflict of interest regarding the publication of this paper.

FUNDING STATEMENT

The study takes partial advantage from analyses (on Mexican samples) founded by the European Union's Horizon 2020 'GE-Mex' research and innovation program under the grant agreement number 727550.

APPENDIX A

See Table 5.

Table 5. Summary of measured properties for the tested rocks.

Set	Rock type	T: °C	ρ: kg/m^3	σ_ρ: kg/m^3	ρ_{wet}: kg/m^3	$\sigma_{\rho wet}$: kg/m^3	n: dimensionless	σ_n: dimensionless	V_P: m/s	σ_{VP}: m/s	V_S: m/s	σ_{VS}: m/s	F: dimensionless	σ_F: dimensionless
RLM	Limestone	20	2779	28	2778	28	0·00105	0·00001	5692	184	3220	45	1277	601
		200	2755	17	2736	17	0·00336	0·00003	6209	44	3007	21	1406	326
		400	2811	28	2843	28	0·03203	0·00034	2559	55	1079	40	65	6
		600	2754	21	2818	21	0·06363	0·00047	2267	134	743	22	111	9
Valdieri	Marble	20	2712	15	2714	15	0·00150	0·00002	7500	87	4170	15	1200	148
		105	2712	16	2714	16	0·00221	0·00001	7382	131	4131	19	434	158
		200	2708	17	2712	17	0·00405	0·00002	4264	109	2831	40	228	76
		400	2710	19	2721	19	0·01150	0·00008	2275	34	1529	15	72	6
		600	2619	38	2648	39	0·02854	0·00045	1257	14	865	11	4	2
GQ	Dolomitic marble	20	2647	20	2650	20	0·00528	0·00005	5238	181	2863	23	497	132
		105	2640	30	2648	30	0·00626	0·00006	4482	162	2437	27	242	50
		200	2639	20	2648	20	0·00931	0·00009	3818	181	2087	84	156	18
		400	2632	30	2651	30	0·01856	0·00020	1308	58	782	48	76	13
		600	2618	30	2650	30	0·03273	0·00038	928	35	519	13	24	8
Brazil C	Marble	20	2756	38	2801	38	0·00349	0·00009	5692	211	3151	152	838	237
		200	2751	37	2756	37	0·00506	0·00010	5623	105	3006	16	539	76
		400	2752	38	2762	38	0·00989	0·00019	4528	79	2139	21	271	85
		600	2735	38	2760	38	0·02541	0·00051	1819	136	836	16	146	67
Brazil D	Marble	20	2851	40	2865	40	0·00248	0·00005	5750	644	2884	132	604	144
		200	2853	38	2857	38	0·00392	0·00008	5263	92	2471	76	478	99
		400	2823	38	2831	38	0·00780	0·00014	3736	105	1796	190	290	86
		600	2799	38	2844	39	0·04523	0·00111	1785	85	665	4	146	96
Brazil SJ	Marble	20	2878	39	2881	39	0·00326	0·00006	5780	179	3131	63	862	202
		200	2858	38	2867	38	0·00834	0·00011	4804	54	2335	30	252	23
		400	2853	38	2864	38	0·01117	0·00016	3931	53	1627	68	189	17
		600	2884	38	2917	39	0·03270	0·00045	1355	6	808	9	162	13

REFERENCES

Ara, T. S., Talabani, S., Atlas, B., Vaziri, H. H. & Islam, M. R. (2001). In-depth investigation of the validity of the Archie equation in carbonate rocks. In *Proceedings – SPE production operations symposium, Oklahoma City, Oklahoma*, pp. 177–183, https://doi.org/10.2523/67204-ms.

Archie, G. E. (1942). The electrical resistivity log as an aid in determining some reservoir characteristics. *Trans. Am. Inst. Mech. Engrs* **146**, No. 1, 54–67.

Arganda-Carreras, I., Fernández-González, R., Muñoz-Barrutia, A. & Ortiz-De-Solorzano, C. (2010). 3D Reconstruction of histological sections: application to mammary gland tissue. *Microsc. Res. Technol.* **73**, No. 11, 1019–1029, https://doi.org/10.1002/jemt.20829.

ASTM (2008). D 2845-08: Standard test method for laboratory determination of pulse velocities and ultrasonic elastic constants of rock (withdrawn 2017), ASTM International, West Conshohocken, PA, USA.

Brotóns, V., Tomás, R., Ivorra, I. & Alarcón, J. C. (2013). Temperature influence on the physical and mechanical properties of a porous rock: San Julian's calcarenite. *Engng Geol.* **167**, 117–127, https://doi.org/10.1016/j.enggeo.2013.10.012.

Castagna, A., Ougier-Simonin, A., Benson, P. M., Browning, J., Walker, R. J., Fazio, M. & Vinciguerra, S. (2018). Thermal damage and pore pressure effects of the brittle-ductile transition in Comiso limestone. *J. Geophys. Res. Solid Earth* **123**, No. 9, 7644–7660, https://doi.org/10.1029/2017JB015105.

Dwivedi, R. D., Goel, R. K., Prasad, V. V. R. & Sinha, A. (2008). Thermo-mechanical properties of Indian and other granites. *Int. J. Rock Mech. Min. Sci.* **45**, No. 3, 303–315, https://doi.org/10.1016/j.ijrmms.2007.05.008.

Ferrero, A. M. & Marini, P. (2000). Experimental studies on the mechanical behaviour of two thermal cracked marbles. *Rock Mech. Rock Engng* **34**, No. 1, 57–66.

Heap, M. J., Mollo, S., Vinciguerra, S., Lavallée, Y., Baud, P., Dingwell, D. B., Iezzi, G. & von Aulock, F. W. (2013). Thermal weakening of the carbonate basement under Mt. Etna volcano (Italy): implications for volcano instability. *J. Volc. Geother. Res.* **250**, 42–60.

ISRM (1979). Suggested methods for determining water content, porosity, density absorption and related properties and swelling and slake-durability index properties. *Int. J. Rock Mech. Min. Sci.* **16**, 141–156, https://doi.org/10.1016/0148-9062(79)91453-0.

Koca, M. Y., Ozden, G., Yavuz, A. B., Kincal, C., Onargan, T. & Kucuk, K. (2006). Changes in the engineering properties of marble in fire-exposed columns. *Int. J. Rock Mech. Min. Sci.* **43**, No. 4, 520–530, https://doi.org/10.1016/j.ijrmms.2005.09.007.

Musso, G., Cosentini, R. M., Foti, S., Comina, C. & Capasso, G. (2015). Assessment of the structural representativeness of sample data sets for the mechanical characterization of deep formations. *Geophysics* **80**, No. 5, D441–D457, https://doi.org/10.1190/GEO2014-0351.1.

Peng, J., Rong, G., Cai, M., Yao, M. D. & Zhou, C. B. (2016). Physical and mechanical behaviours of a thermal-damaged coarse marble under uniaxial compression. *Engng Geol.* **200**, 88–93.

Schneider, C. A., Rasband, W. S. & Eliceiri, K. W. (2012). NIH Image to ImageJ: 25 years of image analysis. *Nat. Methods* **9**, No. 7, pp. 671–675, https://doi.org/10.1038/nmeth.2089.

Sengun, N. (2013). Influence of thermal damage on the physical and mechanical properties of carbonate rocks. *Arabian J. Geosci.* **7**, 5543–5514, https://doi.org/10.1007/s12517-013-1177-x.

Su, H., Jing, H., Yin, Q. & Yu, L. (2018). Effect of thermal environment on the mechanical behaviors of building marble. *Adv. Civil Engng*, **2018**, 1326503, https://doi.org/10.1155/2018/1326503.

Talabani, S., Boyd, D., El Wazeer, F. & Al Arfi, S. (2000). Validity of Archie equation in carbonate rocks. In *Society of petroleum engineers – Abu Dhabi international petroleum exhibition and conference, 2000, ADIPEC 2000, Abu Dhabi, United Arab Emirates*, https://doi.org/10.2523/87302-ms.

Vagnon, F., Colombero, C., Colombo, F., Comina, C., Ferrero, A. M., Mandrone, G. & Vinciguerra, S. C. (2019). Effects of thermal treatment on physical and mechanical properties of Valdieri marble – NW Italy. *Int. J. Rock Mech. Min. Sci.* **116**, 75–86, https://doi.org/10.1016/j.ijrmms.2019.03.006.

Weydt, L. M., Bär, K., Colombero, C., Comina, C., Deb, P., Lepillier, B., Mandrone, G., Milsch, H., Rochelle, C. A., Vagnon, F. & Sass, I. (2018). Outcrop analogue study to determine reservoir properties of the Los Humeros and Acoculco geothermal fields, Mexico. *Adv. Geosci.* **45**, 281–287, https://doi.org/10.5194/adgeo-45-281-2018.

Yavuz, A. B. & Topal, T. (2007). Thermal and salt crystallization effects on marble deterioration: examples from Western Anatolia. *Turkey Engng Geo.* **90**, No. 1–2, 30–40.

Yavuz, H., Demirdag, S. & Caran, S. (2010). Thermal effect on the physical properties of carbonate rocks. *Int. J. Rock Mech. Min. Sci.* **47**, No. 1, 94–103, https://doi.org/10.1016/j.ijrmms.2009.09.014.

Zhao, Y., Wan, Z., Feng, Z., Yang, D., Zhang, Y. & Qu, F. (2012). Triaxial compression system for rock testing under high temperature and high pressure. *Int. J. Rock Mech. Min. Sci.* **52**, 132–138, https://doi.org/10.1016/j.ijrmms.2012.02.011.

Zhang, W., Sun, Q., Zhu, S. & Wang, B. (2017). Experimental study on mechanical and porous characteristics of limestone affected by high temperature. *Appl. Therm. Engng* **110**, 356–362, https://doi.org/10.1016/j.applthermaleng.2016.08.194.